



HAL
open science

Effects of coupled dark energy on the Milky Way and its satellites

Camilla Penzo, Andrea V. Macciò, Marco Baldi, Luciano Casarini, Jose Oñorbe, Aaron A. Dutton

► To cite this version:

Camilla Penzo, Andrea V. Macciò, Marco Baldi, Luciano Casarini, Jose Oñorbe, et al.. Effects of coupled dark energy on the Milky Way and its satellites. *Monthly Notices of the Royal Astronomical Society*, 2016, 461, pp.2490-2501. 10.1093/mnras/stw1502 . insu-03713168

HAL Id: insu-03713168

<https://insu.hal.science/insu-03713168>

Submitted on 4 Jul 2022

HAL is a multi-disciplinary open access archive for the deposit and dissemination of scientific research documents, whether they are published or not. The documents may come from teaching and research institutions in France or abroad, or from public or private research centers.

L'archive ouverte pluridisciplinaire **HAL**, est destinée au dépôt et à la diffusion de documents scientifiques de niveau recherche, publiés ou non, émanant des établissements d'enseignement et de recherche français ou étrangers, des laboratoires publics ou privés.

Effects of coupled dark energy on the Milky Way and its satellites

Camilla Penzo,^{1,2}★† Andrea V. Macciò,^{3,2} Marco Baldi,^{4,5,6} Luciano Casarini,⁷
Jose Oñorbe² and Aaron A. Dutton^{3,2}

¹Laboratoire Univers et Théories, UMR 8102 CNRS, Observatoire de Paris, Université Paris Diderot, 5 Place Jules Janssen, F-92190 Meudon, France

²Max-Planck-Institut für Astronomie, Königstuhl 17, D-69117 Heidelberg, Germany

³New York University Abu Dhabi, PO Box 129188 Abu Dhabi, UAE

⁴Dipartimento di Astronomia, Università di Bologna, via Ranzani 1, I-40127 Bologna, Italy

⁵INAF - Osservatorio Astronomico di Bologna, via Ranzani 1, I-40127 Bologna, Italy

⁶INFN - Sezione di Bologna, viale Berti Pichat 6/2, I-40127 Bologna, Italy

⁷Departamento de Física, Universidade Federal do Espírito Santo, Av. Fernando Ferrari 514, 29075-910 Vitória (ES), Brazil

Accepted 2016 June 21. Received 2016 May 17; in original form 2015 April 28

ABSTRACT

We present the first numerical simulations in coupled dark energy cosmologies with high enough resolution to investigate the effects of the coupling on galactic and subgalactic scales. We choose two constant couplings and a time-varying coupling function and we run simulations of three Milky Way-sized haloes ($\sim 10^{12} M_{\odot}$), a lower mass halo ($6 \times 10^{11} M_{\odot}$) and a dwarf galaxy halo ($5 \times 10^9 M_{\odot}$). We resolve each halo with several million dark matter particles. On all scales, the coupling causes lower halo concentrations and a reduced number of substructures with respect to Λ cold dark matter (Λ CDM). We show that the reduced concentrations are not due to different formation times. We ascribe them to the extra terms that appear in the equations describing the gravitational dynamics. On the scale of the Milky Way satellites, we show that the lower concentrations can help in reconciling observed and simulated rotation curves, but the coupling values necessary to have a significant difference from Λ CDM are outside the current observational constraints. On the other hand, if other modifications to the standard model allowing a higher coupling (e.g. massive neutrinos) are considered, coupled dark energy can become an interesting scenario to alleviate the small-scale issues of the Λ CDM model.

Key words: methods: numerical – galaxies: evolution – galaxies: formation – galaxies: haloes – dark energy – dark matter.

1 INTRODUCTION

Since the discovery of the accelerated expansion of the universe (Riess et al. 1998; Perlmutter et al. 1999), a cosmological constant Λ has been the most widely accepted explanation for the required negative pressure. Together with cold dark matter, today the dark sector is accounting for about 95 per cent of the total energy density (Planck Collaboration XIII 2015) and builds the foundations for the so-called Λ cold dark matter (Λ CDM) model.

Despite the highly successful inflationary Λ CDM paradigm, the fundamental problems associated with the introduction of a cosmological constant, namely *fine-tuning* and *coincidence* problems (Weinberg 1989), have served as motivations for alternative descriptions of the dark sector. Introducing a time evolving scalar

field (dark energy) responsible for the negative pressure is the approach of quintessence models (Peebles & Ratra 1988; Wetterich 1988) and has been one of the most popular generalizations for the cosmological constant in the last decade. Furthermore, given the currently still unknown nature of the dark sector, the possibility of a non-null coupling between dark matter and dark energy has been considered (Wetterich 1995; Anderson & Carroll 1998; Amendola 2000; Billyard & Coley 2000; Amendola & Tocchini-Valentini 2001; Zimdahl, Pavón & Chimento 2001; Farrar & Peebles 2004; Gromov, Baryshev & Teerikorpi 2004). Given that in these models dark matter and dark energy density evolutions are strongly coupled, this would in turn alleviate the *coincidence* problem (Mangano, Miele & Pettorino 2003; Matarrese, Pietroni & Schimd 2003). The effects of such interaction might be seen on the cosmic microwave background (CMB), on supernovae and on the growth of structures, as pointed out by Matarrese et al. (2003), Amendola (2004), Amendola, Gasperini & Piazza (2004), Koivisto (2005), Guo, Ohta & Tsujikawa (2007) and many others. Structure formation has also been investigated via numerical simulations

* Fellow of the International Max Planck Research School for Astronomy and Cosmic Physics at the University of Heidelberg.

† E-mail: camilla.penzo@obspm.fr

by Macciò et al. (2004), Baldi et al. (2010), Li & Barrow (2011), Carlesi et al. (2014) and their follow up works, where the statistical distribution of structures has been studied. Both Baldi et al. (2010) and Carlesi et al. (2014) found that, when introducing a coupling between dark energy and dark matter, halo concentrations decrease.

In this work, we run the first high-resolution simulations on galactic scales in coupled dark energy cosmologies. Our aim is to obtain high enough resolutions to investigate the properties of the dark matter distribution at subgalactic scales, mass scales at which the effects of the coupling have not yet been studied. The subhaloes that we are interested in will in turn be the hosts of dwarf galaxies and their properties can be compared with observations of satellite dwarf galaxies of both Milky Way and Andromeda. In fact, despite Λ CDM predictions on large scales being in very good agreement with galaxy clustering surveys (Jones et al. 2009; Alam et al. 2015), on galactic scales challenges between Λ CDM predictions and observations have appeared.

First, the *missing satellites* problem, i.e. overabundance of substructures in Λ CDM Milky Way-sized halo simulations when compared to observations of the Milky Way dwarf galaxies (Klypin et al. 1999; Moore et al. 1999). On the other hand, as showed in Madau, Diemand & Kuhlen (2008) and Macciò et al. (2010), accounting for the baryonic physics drastically reduces the number of visible satellites. Secondly, the *core/cusp* problem, namely the inconsistency between the constant density cores estimated from observations and the cuspy inner density profiles found in Λ CDM simulations. See Flores & Primack (1994), Moore (1994), Diemand et al. (2005), Gentile et al. (2009), Walker & Peñarrubia (2011), Agnello & Evans (2012) and Salucci et al. (2012), but also van den Bosch & Swaters (2001), Swaters et al. (2003) and Simon et al. (2005). While this inconsistency can be attributed to baryonic feedback processes (e.g. Governato et al. 2012; Di Cintio et al. 2014; Oñorbe et al. 2015), for the case of Milky Way satellites the baryonic explanation is not straightforward since these objects can be almost completely dark matter dominated. Baldi et al. (2010) and Carlesi et al. (2014) showed that for haloes with $M \gtrsim 10^{13} M_{\odot}$, the coupling between dark matter and dark energy produces density profiles that are less cuspy in the inner density regions, which can help alleviating the core/cusp problem. The aim of this work is to investigate whether this effect persists at much lower masses. Moreover, concentrations of the most massive subhaloes orbiting around a Λ CDM Milky Way-sized halo seem to be too high to be hosting the brightest dwarf galaxies observed. This translates into a prediction from Λ CDM numerical simulations for the existence of massive dark matter subhaloes that seem to have failed at forming stars, and is known as the *too big to fail* problem (Boylan-Kolchin, Bullock & Kaplinghat 2011; Lovell et al. 2012; Rashkov et al. 2012; Tollerud et al. 2012).

Whether these issues bring serious challenges for the Λ CDM model or whether they can entirely be treated by invoking baryonic physics is currently under debate. With this work, we aim at studying the properties of haloes and their substructures to determine whether coupled dark energy cosmologies can alleviate the aforementioned issues. In Section 2, we summarize the theoretical model behind coupled dark energy and we specify our choices of coupling functions. In Section 3, we described the numerical methods used to produce initial conditions and the N -body codes to run the simulations. In Section 4 we show our simulations results, for both haloes and subhaloes. Finally, in Section 5 we present our conclusions.

2 COSMOLOGICAL MODELS

We present a study focused on understanding the non-linear effects of coupled dark energy models on galactic scales. The models that we consider allow for an interaction between dark matter and dark energy (Amendola 2000; Billyard & Coley 2000; Zimdahl et al. 2001; Gromov et al. 2004; Macciò et al. 2004; Baldi et al. 2010) and obey the following lagrangian density:

$$\mathcal{L} = R - \frac{1}{2} \partial^{\mu} \partial_{\mu} \phi - V(\phi) - m(\phi) \bar{\psi} \psi + \mathcal{L}_{\text{kin}}[\psi], \quad (1)$$

where the mass $m(\phi)$ of the dark matter field ψ is a function of the dark energy scalar field ϕ , the $\mathcal{L}_{\text{kin}}[\psi]$ term includes the kinetic part of the dark matter lagrangian density, and we use units in which the reduced Planck mass is assumed to be unity, $M_{\text{Pl}} \equiv 1/\sqrt{8\pi G} = 1$. The choice of $m(\phi)$ specifies the coupling and in our work we use

$$m(\phi) = m_0 e^{-\beta(\phi)\phi}, \quad (2)$$

where m_0 is the mass at $z = 0$ and $\beta(\phi)$ is the coupling function. The respective continuity equations for cold dark matter and dark energy are

$$\begin{aligned} \dot{\rho}_c + 3H\rho_c &= -\beta(\phi)\dot{\phi}\rho_c, \\ \dot{\rho}_{\phi} + 3H\rho_{\phi} &= +\beta(\phi)\dot{\phi}\rho_c, \end{aligned} \quad (3)$$

where ρ_c is the cold dark matter density and ρ_{ϕ} is the dark energy density, which is $\rho_{\phi} \equiv \frac{1}{2}\dot{\phi}^2 + V(\phi)$, $H \equiv \dot{a}/a$ is the Hubble parameter and dots indicate time derivatives. Our choice for the self-interacting dark energy potential is $V(\phi) \propto e^{-\alpha\phi}$, with $\alpha = 0.08$.

The evolution of cold dark matter density perturbations δ_c is regulated by the following equation:

$$\ddot{\delta}_c + (2H - \beta\dot{\phi})\dot{\delta}_c - \frac{3}{2}H^2 [(1 + 2\beta^2)\Omega_c\delta_c + \Omega_b\delta_b] = 0, \quad (4)$$

where δ_b are the baryonic matter density perturbations, Ω_c and Ω_b are, respectively, the density parameters $\Omega_i \equiv \rho_i/\rho_{\text{crit}}$ for cold dark matter and baryons, with critical density $\rho_{\text{crit}} = 3H^2/8\pi G$ and G Newton's constant. Two extra terms appear in equation (4) compared to the Λ CDM case: a friction term $-\beta\dot{\phi}\dot{\delta}_c$ and the factor $(1 + 2\beta^2)$ responsible for the enhancement of the gravitational force acting on cold dark matter particles, which is known as 'fifth force'. As pointed out in Baldi (2011b), in the linear regime both these extra terms produce an acceleration of growth of cold dark matter density perturbations. On the other hand, when considering the non-linear effects, the friction term is responsible for lowering the concentration of dark matter haloes.

The appearance of extra terms becomes clear when calculating the acceleration felt by the i th dark matter particle \vec{v}_i in a coupled dark energy cosmology for the limit of a light scalar field (see Baldi et al. 2010 for calculation):

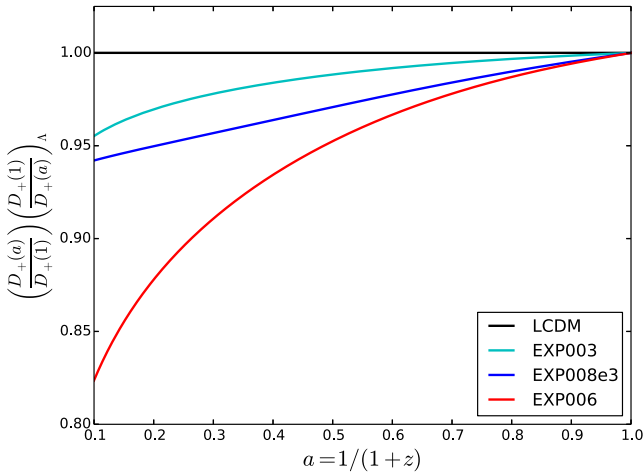
$$\ddot{\vec{v}}_i = \beta(\phi)\dot{\phi}\vec{v}_i + G[1 + 2\beta(\phi)^2] \sum_{j \neq i} \frac{m_j \mathbf{r}_{ij}}{|\mathbf{r}_{ij}|^3}, \quad (5)$$

where \vec{v}_i is the velocity of the i th dark matter particle, m_j is the mass of the j th particle and \mathbf{r}_{ij} is the distance between the i th and the j th dark matter particles. The term $\beta(\phi)\dot{\phi}\vec{v}_i$ accelerates dark matter particles in the direction of their motion and thus lowers halo concentrations.

Based on Baldi et al. (2010); Baldi (2011b), we chose three coupling scenarios. EXP003 and EXP006 have a constant coupling with $\beta = 0.15, 0.3$, while EXP008e3 has a variable coupling $\beta(\phi)$ (see Table 1 for more details). The coupling values for EXP003 and

Table 1. A summary of the cosmological models considered in this work with their basic parameters.

Model	Potential	α	$\beta(\phi)$
Λ CDM	$V(\phi) = A$	–	–
EXP003	$V(\phi) = Ae^{-\alpha\phi}$	0.08	0.15
EXP008e3	$V(\phi) = Ae^{-\alpha\phi}$	0.08	$0.4\exp[3\phi]$
EXP006	$V(\phi) = Ae^{-\alpha\phi}$	0.08	0.3

**Figure 1.** Linear growth factor evolutions for all cosmologies normalized to today's values divided by the Λ CDM evolution.

EXP008e3 are within the CMB constraints found in Pettorino et al. (2012), while the coupling value for EXP006 represents an extreme case (about 6σ outside observational limits from Pettorino et al. 2012) which is used as a toy model to better investigate the effects of the coupling on non-linear structure formation.

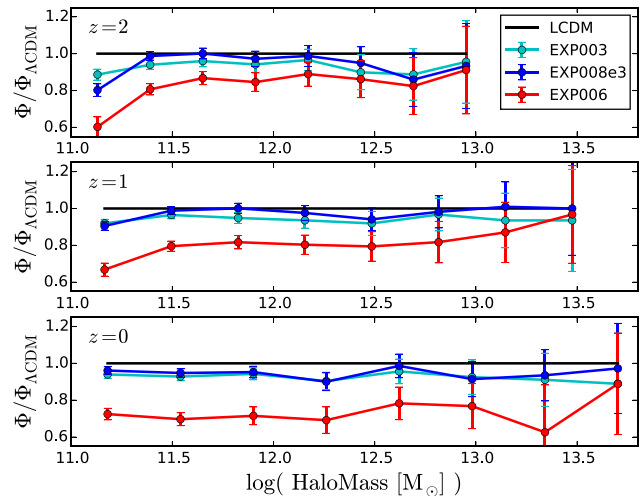
3 NUMERICAL METHODS

3.1 Initial conditions and coupled dark energy

As in Penzo et al. (2014), we used GRAFIC-DE, an extension of the initial condition generator GRAFIC-2 (Bertschinger 2001) such that initial conditions for a generic cosmological model can be produced once the evolution of the cosmological parameters are given as an input. GRAFIC-DE requires transfer functions, evolution of the density parameters Ω_i , linear growth factor D_+ and growth rate $f_{\text{DE}} \equiv d \ln D_+ / d \ln a$. As the original code, GRAFIC-DE is able to generate multimass initial conditions from a cosmological box. In Fig. 1, we show the evolution of the linear growth factor D_+ for all four cosmological models. The transfer functions for Λ CDM have been produced using CAMB (Lewis & Bridle 2002), while the transfer functions for the coupled dark energy models T_{cDE} have been produced by scaling the Λ CDM transfer functions T_{Λ} with the D_+ of the coupled model, i.e. $T_{\text{cDE}} = T_{\Lambda} D_{+\text{cDE}} / D_{+\Lambda}$. All initial conditions were created using the same random seeds, in order to be able to compare structures among the models. We chose to normalize all the cosmological models so that they share the same cosmological parameters at $z = 0$: $\Omega_{\text{b}0} = 0.0458$, $\Omega_{\text{DM}0} = 0.229$, $H_0 = 70.2 \text{ km s}^{-1} \text{ Mpc}^{-1}$, $\sigma_8 = 0.816$, $n_s = 0.968$, where these parameters are density parameters for baryons and dark matter, Hubble constant, root mean square of the fluctuation amplitudes and primeval spectra index. The reason for this choice is that in this work we are not interested in

Table 2. Physical properties of the five haloes in all cosmologies, Λ CDM, EXP003, EXP008e3 and EXP006. We show mass at R_{200} , R_{200} , concentrations and number of particles within R_{200} .

	M_{200} (M_{\odot})	R_{200} (kpc)	$c \equiv R_{200}/r_s$	N_{200}
<i>Haloα</i>				
Λ CDM	2.6×10^{12}	284	11.8	6.8×10^6
EXP003	2.5×10^{12}	281	9.1	6.6×10^6
EXP008e3	2.6×10^{12}	282	10.2	6.7×10^6
EXP006	2.1×10^{12}	265	4.6	5.5×10^6
<i>Haloβ</i>				
Λ CDM	2.5×10^{12}	278	10.7	6.3×10^6
EXP003	2.2×10^{12}	267	8.0	5.7×10^6
EXP008e3	2.2×10^{12}	268	8.7	5.8×10^6
EXP006	1.7×10^{12}	246	4.3	4.5×10^6
<i>Haloγ</i>				
Λ CDM	9.7×10^{11}	204	10.8	1.0×10^7
EXP003	9.3×10^{11}	201	8.6	9.9×10^6
EXP008e3	9.5×10^{11}	203	9.6	1.0×10^7
EXP006	7.6×10^{11}	188	3.2	8.1×10^6
<i>Haloδ</i>				
Λ CDM	6.4×10^{11}	177	13.3	6.8×10^6
EXP003	5.6×10^{11}	170	9.7	6.0×10^6
EXP008e3	5.9×10^{11}	172	11.0	6.3×10^6
EXP006	5.3×10^{11}	166	4.7	5.6×10^6
<i>Haloϵ</i>				
Λ CDM	4×10^9	33	15.3	3.1×10^6
EXP006	3×10^9	30	6.6	2.4×10^6

**Figure 2.** Ratio between the mass functions for the coupled dark energy cosmologies and the one from Λ CDM for redshifts $z = 2, 1, 0$ for the cosmological boxes of size $80 \text{ Mpc } h^{-1}$.

the cosmological viability of these models *per se*, but rather on the effects at non-linear scales. With this choice of normalization, we are able to isolate the effects of the coupling on non-linear structure formation from the effects of different cosmological parameters at $z = 0$.

3.2 N -body simulations

We first generate two sets of uniform particle distributions, a $80 \text{ Mpc } h^{-1}$ box and a $12 \text{ Mpc } h^{-1}$ box, both with 350^3 particles.

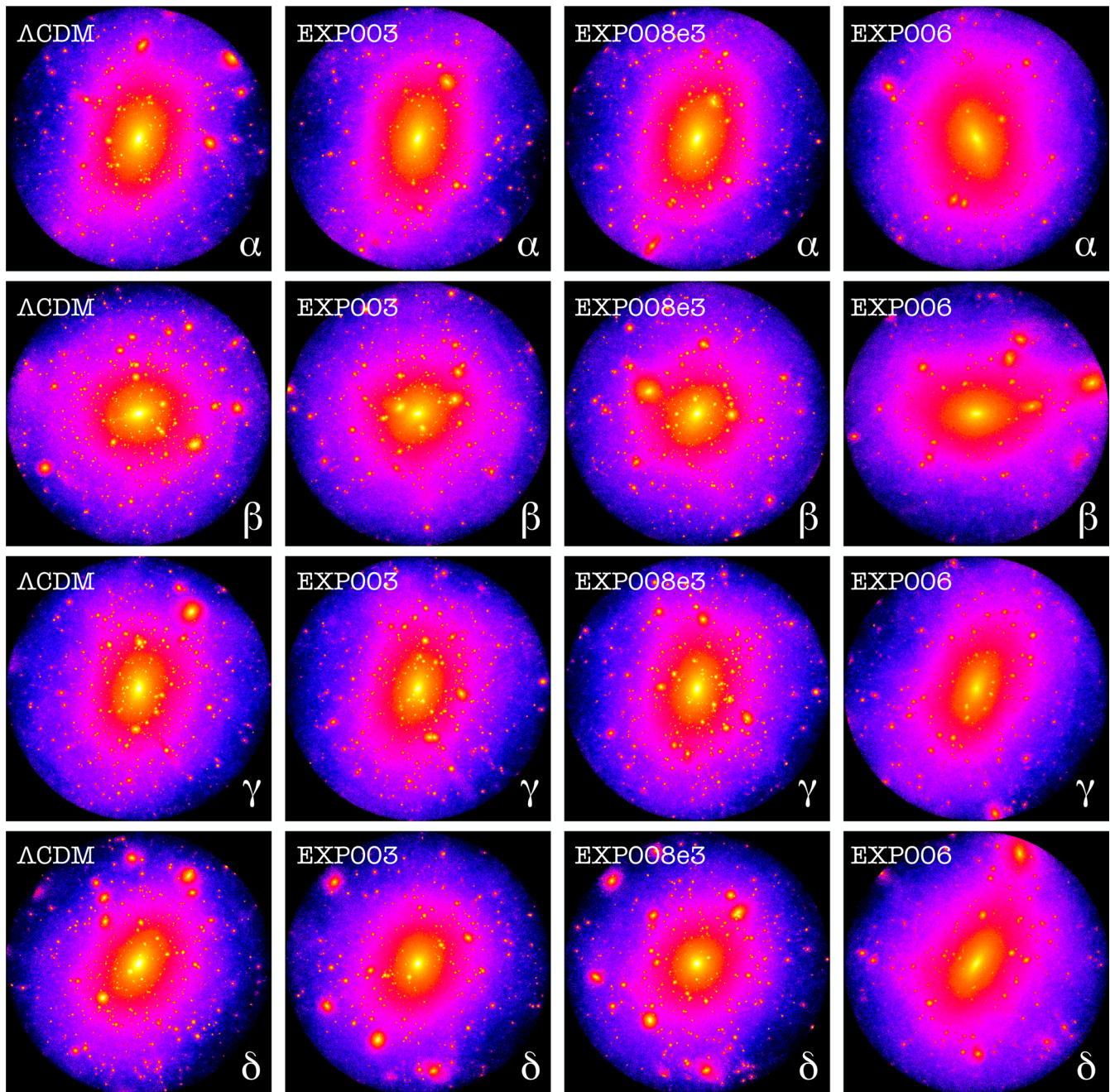


Figure 3. Projected density maps of our sample at $z = 0$. From first row to last we are showing halo α , halo β , halo γ , halo δ ; from first column to last we are showing Λ CDM, EXP003, EXP008e3 and EXP006 cosmologies. All images are spheres of radius R_{200} , radius at which the density is equal to 200 times the critical density.

The initial conditions were evolved with the code `GADGET-2` (Springel 2005), which includes the coupled dark energy implementation introduced in Baldi et al. (2010).

We chose four dark matter haloes in the Λ CDM $80 \text{ Mpc } h^{-1}$ box and one dwarf halo in the Λ CDM $12 \text{ Mpc } h^{-1}$ box, and looked for their corresponding realizations in the coupled dark energy simulations. Note that we used the same random seed for all initial conditions to be able to follow the same haloes in all cosmological boxes. Our haloes have been chosen so that no other haloes with comparable masses were found within four times their virial radii. We then re-ran the cosmological boxes with increased resolution in

a Lagrangian volume that includes all particles that at $z = 0$ were found in three times virial radii of each selected halo.

Our final sample is composed of three Milky Way-sized haloes (halo α , halo β and halo γ), a $6 \times 10^{11} M_{\odot}$ halo (halo δ) and a dwarf halo (halo ϵ). For more details on the haloes properties at $z = 0$, see Table 2. For the halo identification, we used the code Amiga Halo Finder (AHF; Knollmann & Knebe 2009). When using AHF we are not taking into account the change in the gravitational constant (which is instead included in the modified version of `GADGET-2` that we used for all our simulations). We believe this does not significantly influence the halo identification process since the effect of the change in the

gravitational constant is non-significant at non-linear scales; this is shown in the analysis carried out in Baldi (2011b).

The softening lengths are chosen to be 1/40 of the intraparticle distance in the low-resolution simulation divided by the refinement factor RF; RF = 15 for halo α , halo β and halo ϵ , RF = 24 for halo γ and halo δ . Precisely, the softening lengths are 0.54 kpc for halo α and halo β , 0.34 kpc for halo γ and halo δ , 0.081 kpc for halo ϵ . The particle masses at $z = 0$ in the high-resolution volumes are $3.8 \times 10^5 M_\odot$ for halo α and halo β , $9.4 \times 10^4 M_\odot$ for halo γ and halo δ , $1.3 \times 10^3 M_\odot$ for halo ϵ . In Fig. 3, we show the projected density maps of the four most massive haloes for each cosmological model. We will discuss the dwarf halo in Section 4.3. For the density maps and throughout the paper, we chose to calculate halo properties using R_{200} , radius at which the density is 200 times the critical density.

4 RESULTS

Fig. 2 shows the ratio between the mass functions for the coupled dark energy cosmologies with the one for Λ CDM for redshifts $z = 2, 1, 0$ for our 80 Mpc h^{-1} boxes. For all redshifts, significant differences on the mass functions are only present in EXP006 (red lines). The higher the coupling the lower the number of haloes at a given mass. This behaviour is what Baldi et al. (2010) found for higher halo masses. In their work, they have a box size of $320h^{-1}$ Mpc which limits the study to haloes with masses $M \gtrsim 10^{13} M_\odot$. For this reason, in our work we focus on testing the effects of the coupling at lower halo masses. In Section 2, we briefly described the coupled dark energy cosmological model and the appearance of extra terms introduced by the coupling. Baldi (2011b) shows that the term affecting structure formation the most is the friction term of equation (5). By accelerating dark matter particles in the direction of their motion, the kinetic energy of the system will increase and the system itself will react by expanding. As a consequence, Baldi (2011b) shows that part of the mass is pushed at greater radii and the halo masses decrease. In the following sections, we will show how the effects of the extra terms is key to explain the differences from Λ CDM for both main haloes and their subhaloes for the case of Milky Way-sized haloes.

4.1 Host haloes properties

In the 80 Mpc h^{-1} boxes at $z = 0$, we choose four haloes, halo α , halo β , halo γ and halo δ , and we resimulated them with much higher resolutions. We checked that all four haloes are relaxed using the criterion from Macciò, Dutton & van den Bosch (2008). In the following sections, we show their concentrations and density profiles, rotation curves, evolution of the scale radius and accretion histories.

4.1.1 Concentrations and density profiles

By introducing a coupling between dark matter and dark energy, halo concentrations decrease. This was shown in Baldi et al. (2010), Li & Barrow (2011), and Carlesi et al. (2014) for haloes with masses $M \gtrsim 10^{13} M_\odot$. In this work, we investigate mass scales $M \lesssim 10^{12} M_\odot$. Furthermore, the resolution that we are able to reach is higher thanks to the multimass technique. In Table 2, we show the concentration values for each halo, for which we use the definition

$$c \equiv R_{200}/r_s, \quad (6)$$

where r_s is the scale radius in the Navarro–Frenk–White (NFW) profile (Navarro, Frenk & White 1997). We computed r_s via a χ^2

minimization procedure using the Levenberg & Marquart method as in Macciò et al. (2008). In agreement with literature, we find that haloes which live in a coupled dark energy cosmology have lower concentrations. Fig. 4 shows the density profiles for halo α , halo β , halo γ and halo δ . The ordering of the profiles with respect to Λ CDM is maintained for all four haloes, with a significant flattening of the inner part of the profiles only for the extreme coupled cosmology EXP006, while differences are less evident in the EXP003 and EXP008e3 haloes. Interestingly, the EXP006 realization of halo γ ($M = 7.6 \times 10^{11} M_\odot$) produces a much flatter halo profile, with slope $\alpha = -0.8$, which falls out of NFW parametrization. On the other hand, all other profiles of halo α , halo β , halo γ and halo δ in all cosmologies are well described by the NFW profile. Additionally, in Fig. 5 we show the rotation curves at $z = 0$ for the four haloes. Note that, due to the high resolution of our simulations, the errors $\sqrt{N_p}$ are well below 1 per cent everywhere, with N_p number of particles for each bin. For models within the observational constraints, the rotation curves are not significantly affected. The only case in which we observe a considerable flattening is the extreme model EXP006, for all four cases. This is in agreement with Penzo et al. (2014), where we find that differences in rotation curves among models within observational constraints for dynamical dark energy are not significant in the dark matter only case. On the contrary, in hydrodynamical simulations we find observable differences in rotation curves due to the effects of baryons which enhance the variations in the dark matter accretion. We expect the same enhancement also in coupled dark energy models once hydrodynamics is taken into account. This aspect will be explored in a future work.

In the analysis carried out in Baldi (2011a,b), lower concentrations (and therefore less steep density profiles and flatter rotation curves) were shown to be linked to the presence of the friction term $-\beta\dot{\phi}\delta_c$ in the equation for the linear evolution of density perturbations (equation 4), which injects kinetic energy into the halo. The resulting expansion lowers halo concentration by moving matter from inner to outer radii. As a consequence, rotation curves tend to be flatter than in Λ CDM and density profiles less centrally concentrated. We suggest that the same mechanism is in place also for the less massive haloes ($M \lesssim 10^{12} M_\odot$) analysed in this work. We are aware that the mass range is different to the one probed by Baldi (2011a,b), and we acknowledge the possibility that other effects could be important at these masses.

4.1.2 NFW scale radius evolution

In the Section 4.1.1, we have showed that haloes that form in a coupled dark energy cosmology with a high value for the coupling constant have concentrations that are significantly lower at $z = 0$. Given that almost all haloes are well described by an NFW density profile, it means that their NFW scale radii r_s are much larger than the scale radii of the corresponding Λ CDM realizations. In Fig. 6, we show the behaviour of the scale radius r_s as a function of redshift for halo β in all four cosmologies; the other Milky Way-sized haloes have similar behaviours. The fitting is performed with the GNPLOT fitting routine and the asymptotic standard error is shown. Compared to the Λ CDM case, haloes which live in coupled dark energy cosmologies show a larger scale radius at all redshifts.

4.1.3 Main haloes accretion histories

In order to better investigate the origin of the different concentrations, in this section we focus on halo formation times. Fig. 7

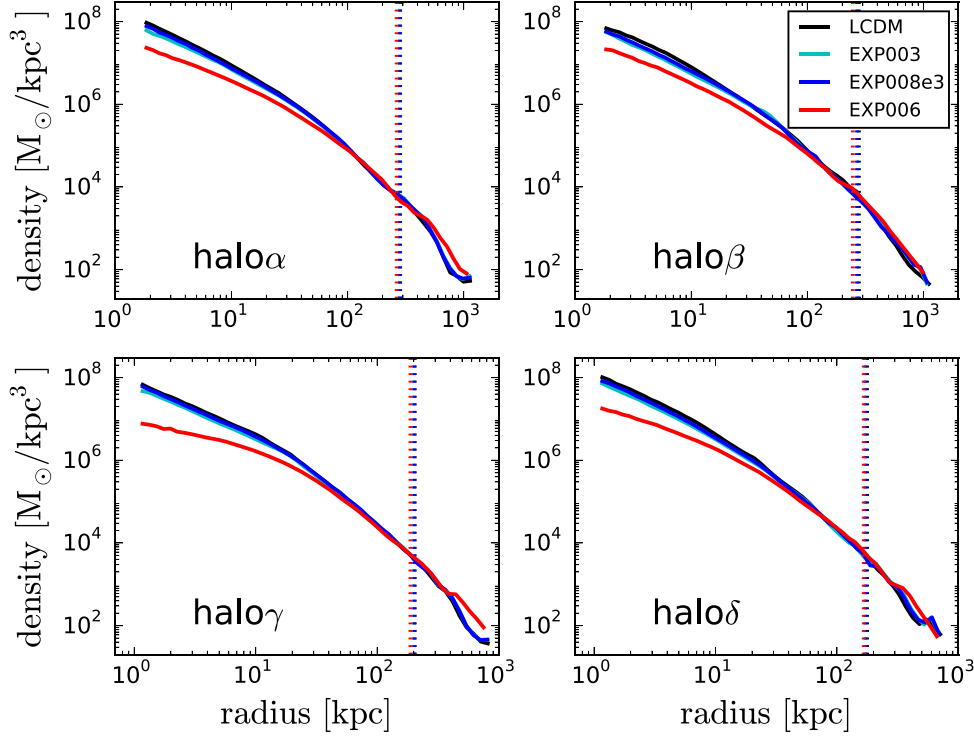


Figure 4. Density profiles for halo α , halo β , halo γ and halo δ at $z = 0$, each for Λ CDM (black), EXP003 (cyan), EXP008e3 (blue) and EXP006 (red). The inner radius is equal to three times the softening length, while the outer radius is four times R_{200} of each halo. The vertical dashed lines mark R_{200} for each halo in each cosmology.

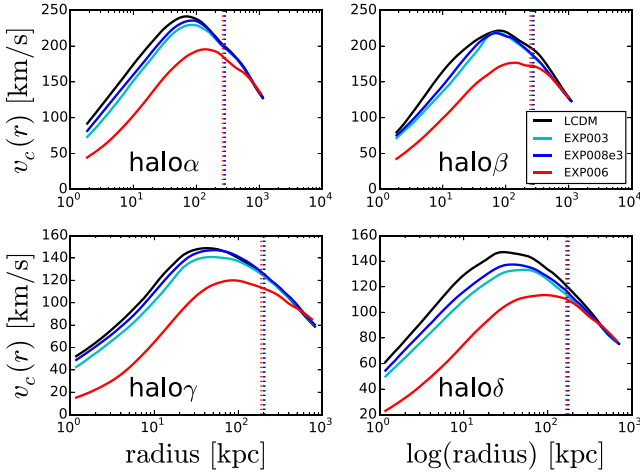


Figure 5. Rotation curves for halo α , halo β , halo γ and halo δ at $z = 0$, each for Λ CDM, EXP003, EXP008e3 and EXP006. The inner radius is equal to three times the softening length, while the outer radius is four times R_{200} of each halo. The vertical dashed lines mark R_{200} for each halo in each cosmology.

shows halo accretion histories, namely the evolution of the mass enclosed in R_{200} as a function of expansion factor $a = 1/(1+z)$. Haloes growing in Λ CDM, EXP003 and EXP008e3 cosmologies show similar accretion histories; while haloes forming in the EXP006 cosmology show a lower clustering compared to Λ CDM starting between $0.4 \lesssim a \lesssim 0.6$ and arriving today with a significantly lower halo mass. Among the three haloes, coupled cosmology runs show unexpected drops in the accretion histories. These would be unusual in a Λ CDM scenario since halo total masses do

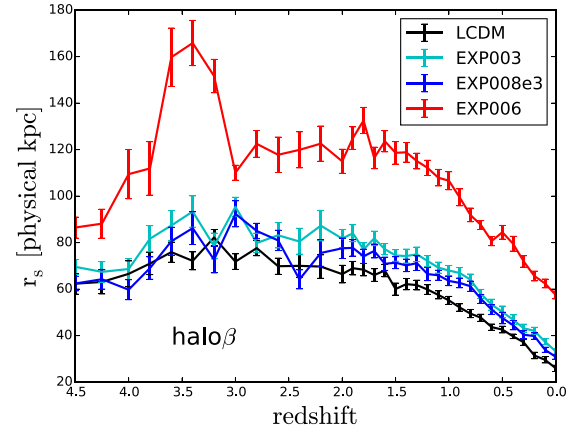


Figure 6. Scale radius obtained by fitting an NFW density profile using the Levenberg & Marquart method for halo β as a function of redshift.

not decrease unless it is a temporary effect of a merger (see for instance halo α and halo β around $a = 0.3$). On the other hand, in coupled cosmologies, by injecting kinetic energy into the system, the friction term in equation (4) moves particles to radii larger than R_{200} and may cause some of them to become gravitationally unbound. These effects of the coupling were previously studied in Baldi (2011a,b).

In order to estimate the time of formation for each halo, we searched for the scale factor at which the halo has gained half of its today's mass. Table 3 summarizes the formation epochs for all haloes. We find that haloes in the EXP006 cosmology do not have later formation times than in Λ CDM. Two of our EXP006 haloes show earlier formation times compared to their Λ CDM halo

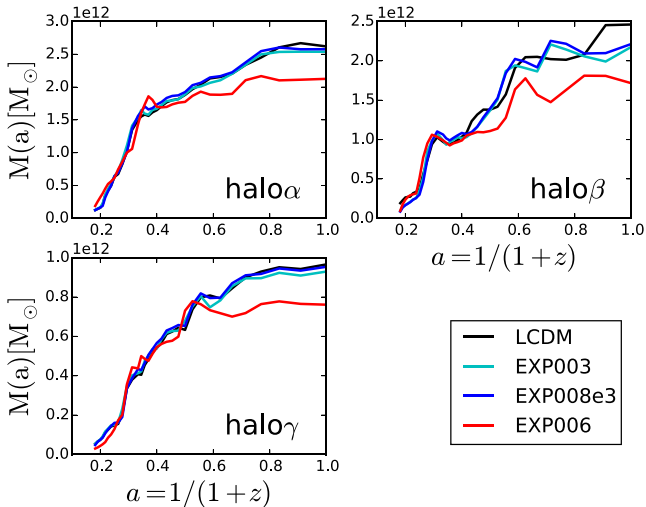


Figure 7. Evolution of the mass enclosed in R_{200} as a function of the scale factor for halo α , halo β , halo γ in all four cosmologies.

Table 3. Values for the formation epochs a_c for halo α , halo β , halo γ in all four cosmologies.

	Λ CDM	EXP003	EXP008e3	EXP006
halo α	0.310	0.304	0.308	0.313
halo β	0.434	0.436	0.438	0.270
halo γ	0.370	0.355	0.361	0.299

counterparts. This is in agreement with that found in Baldi et al. (2010) and Baldi (2011b) for more massive haloes: coupled dark energy cosmologies statistically show earlier formation times than Λ CDM. On the other hand, as pointed out in Wechsler et al. (2002), Ludlow et al. (2013) and Dutton & Macciò (2014), in a Λ CDM cosmology an early formation epoch leads to higher concentrations. The same happens for dynamical dark energy cosmologies, e.g. Klypin et al. (2003) and Dolag et al. (2004). Interestingly, in coupled dark energy cosmologies this behaviour is not preserved. Despite the fact that a stronger coupling can result in an earlier or comparable halo formation epoch, halo concentrations decrease when the coupling is increased. The friction term in equation (4) is responsible for making the halo expand by altering its virial equilibrium through the injection of kinetic energy in the system, which in turn lowers the concentration. This shows how in coupled cosmologies lower concentrations are not the result of formation histories but rather the effect of modified dynamics.

4.2 Subhaloes

In this section, we study the subhalo abundance, their radial distribution and circular velocities.

4.2.1 Abundance

The lower number of substructures present in EXP006 haloes compared to Λ CDM can be recognized in Fig. 3. Fig. 8 shows the subhalo mass function, where only subhaloes that lie within R_{200} and that have more than 400 particles are considered. The errors are taken to be \sqrt{N} , where N is the number of counts in a given mass bin. The total number of subhaloes in EXP006 realizations is always from 50 to 75 per cent lower than in the respective Λ CDM cases,

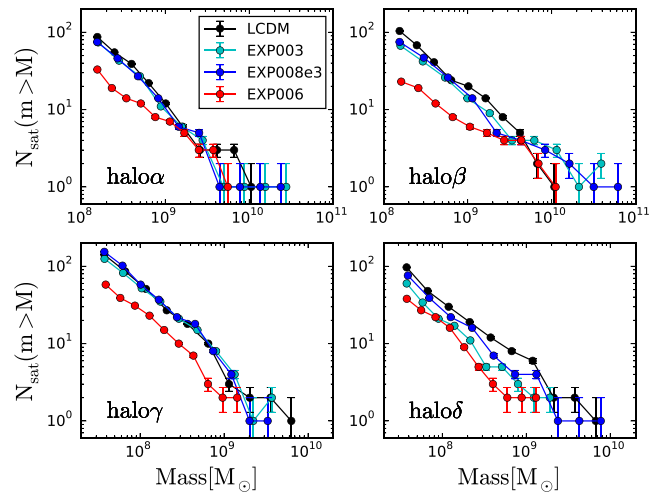


Figure 8. Cumulative number of subhaloes with more than 400 particles as a function of their mass for halo α , halo β , halo γ and halo δ at $z = 0$ for each cosmology.

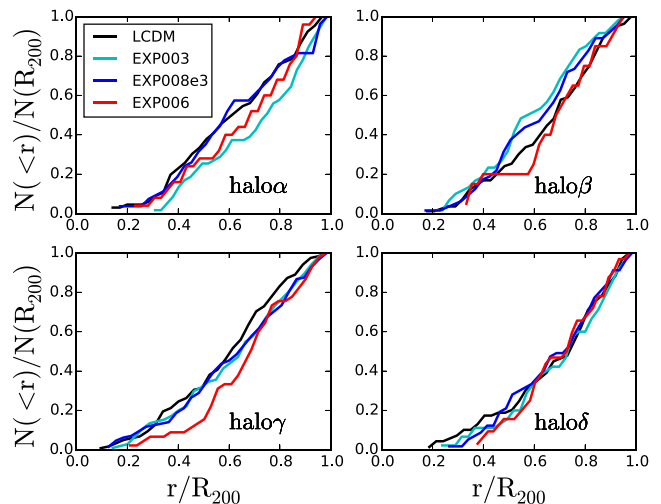


Figure 9. Cumulative number of subhaloes with more than 400 particles as a function of distance from the main halo centre for halo α , halo β , halo γ and halo δ at $z = 0$ for each cosmology.

while differences between EXP003 and EXP008e3 and Λ CDM are much less evident (~ 10 per cent). Thus, the missing satellites problem (Klypin et al. 1999; Moore et al. 1999) can be progressively alleviated when increasing the coupling. Note that the differences in the subhaloes minimum mass among halo α , halo β and halo γ , halo δ are due to the different resolutions used (see Section 3.2).

4.2.2 Radial distribution

Fig. 9 shows the cumulative distribution of subhaloes as a function of the distance from the main halo centre normalized to the total number of subhaloes within R_{200} . All haloes in all cosmologies show non-significant differences in the cumulative radial distribution. In order to better understand the distribution of subhaloes, Fig. 10 shows the differential distribution in a sphere of constant radius for all cosmologies, the radii are 350 kpc for halo α and halo β , 250 kpc for halo γ and 200 kpc for halo δ . The number of bins is kept the same for each halo in all cosmologies and the vertical lines show the virial radii. The distributions show a clear decrease of the number

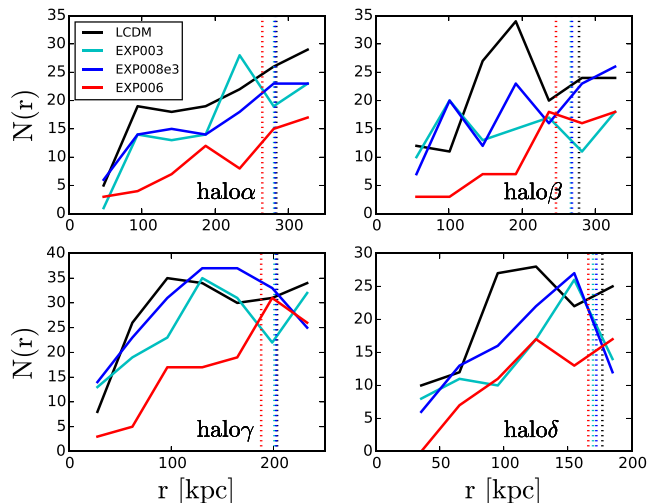


Figure 10. Differential number of subhaloes in R_{200} with more than 400 particles as function of distance from main halo centre for $\text{halo}\alpha$, $\text{halo}\beta$, $\text{halo}\gamma$ and $\text{halo}\delta$ at $z = 0$ for each cosmology. The vertical dashed lines mark R_{200} for each halo in each cosmology. For a given halo, the binning is kept constant for all cosmologies.

of subhaloes in EXP006 haloes compared to their respective Λ CDM cases, while for EXP003 and EXP008e3 cosmologies differences are not so evident.

As pointed out in Section 4.1.3, the extra terms due to the coupling appearing in the equation for the evolution of density perturbations (equation 4) decrease halo concentrations despite the earlier or comparable halo formation epochs. We claim that the decrease of halo concentration can be also responsible for the lower number of subhaloes compared to Λ CDM. Given that also subhaloes have lower concentrations (confirmed by the subhaloes rotation curves shown in Fig. 12), when falling into the main halo potential well, they can be heavily stripped and less subhaloes with more than 400 particles survive. If this claim is correct, we should be able to find a difference in the subhaloes number distribution when we reach distances from the main halo centre that are bigger than the radius from which the gravitational influence of the host halo is felt. In Fig. 11, we show the differential radial distribution of the number of subhaloes out to about three times the virial radius of each halo. For the sake of clarity, we choose to show only Λ CDM and the most extreme case, EXP006, for all four haloes. The dotted lines represent one and two times R_{200} for each halo in each cosmology. What we would like to stress, is that there seem to be a decrease in the number of subhaloes living in EXP006 cosmology compared to their Λ CDM realizations *only* within the gravitational influence of the main halo. Between 1.5 and $2R_{200}$, this behaviour inverts and haloes living in the strongly coupled cosmology seem to have a larger or at least a comparable number of subhaloes with respect to their Λ CDM cases. Thus, we ascribe the presence of a lower subhaloes number to a massive stripping effect rather than EXP006 producing intrinsically a lower number of subhaloes. On the other hand, we cannot exclude that coupled cosmologies could show a lower number of subhaloes because mergers and accretions could be much slower in EXP006, so that subhaloes form more slowly and in smaller numbers, and only fewer of them might have fallen into the main haloes at $z = 0$. Finally, we would like to stress on the fact that lowering the number of subhaloes can also be achieved by warm dark matter (WDM) cosmologies (e.g. Anderhalden et al. 2013), but the fundamental difference lies on the fact that WDM

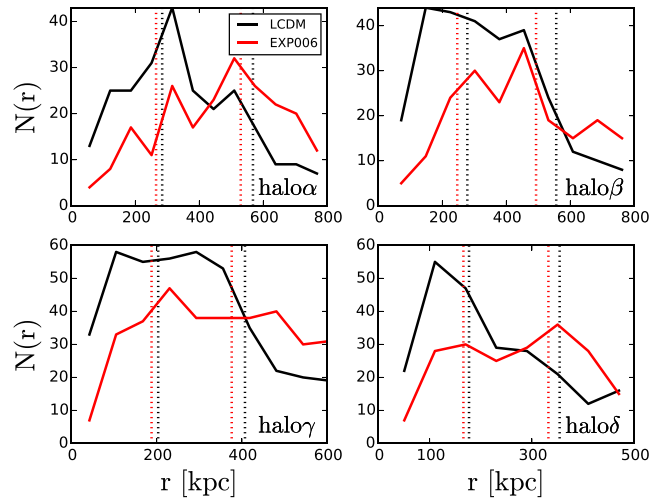


Figure 11. Number of subhaloes in $3R_{200}$ with more than 400 particles as function of distance from main halo centre for $\text{halo}\alpha$, $\text{halo}\beta$, $\text{halo}\gamma$ and $\text{halo}\delta$ at $z = 0$ for each cosmology. The vertical dashed lines mark R_{200} and $2R_{200}$ for each halo. For a given halo, the binning is kept constant for all cosmologies.

will have a lower number of (sub)haloes both inside and *outside* the virial radius, due to the overall suppression of the initial power spectrum. On the contrary, our coupled models have an even larger number of subhaloes compared to Λ CDM outside the virial radius, and this is even true for EXP006. To summarize, subhaloes in WDM cosmologies were never formed, while in coupled dark energy cosmologies subhaloes do form but they could be heavily stripped.

4.2.3 Circular velocities

Boylan-Kolchin et al. (2011) first showed that N -body simulations of a Milky Way-sized halo predict a significant number of subhaloes with circular velocities higher than the circular velocities that we measure for the brightest satellites of the Milky Way, which is surprising since these massive subhaloes should not fail in producing stars.

The discrepancy between Λ CDM prediction and observations can be alleviated in multiple ways, starting from baryonic processes. Brooks & Zolotov (2014) suggest that baryonic feedback processes could be responsible for a dark matter redistribution, with the result of decreasing the central densities of the most massive subhaloes. Rashkov et al. (2012) point out that the possibility of star formation being stochastic below a certain mass would justify the Milky Way having massive dark satellites; furthermore, they highlight the fact that the tension between the Via Lactea II simulation and observations is only a factor of 2 in mass, which suggests that the uncertainty on the Milky Way virial mass could be a viable way out from the tension (Vera-Ciro et al. 2013; Kennedy et al. 2014). Purcell & Zentner (2012) showed that there exists a significant variation in subhalo properties even when the host haloes have the same virial mass.

Last but not least, the discrepancy can be alleviated by appealing to non- Λ CDM cosmologies. The cases for warm, mixed (cold and warm) and self-interacting dark matter are considered in Lovell et al. (2012), Anderhalden et al. (2012, 2013) and Vogelsberger, Zavala & Loeb (2012), respectively. In all cases they find that subhaloes are less concentrated due to their late formation time, suggesting

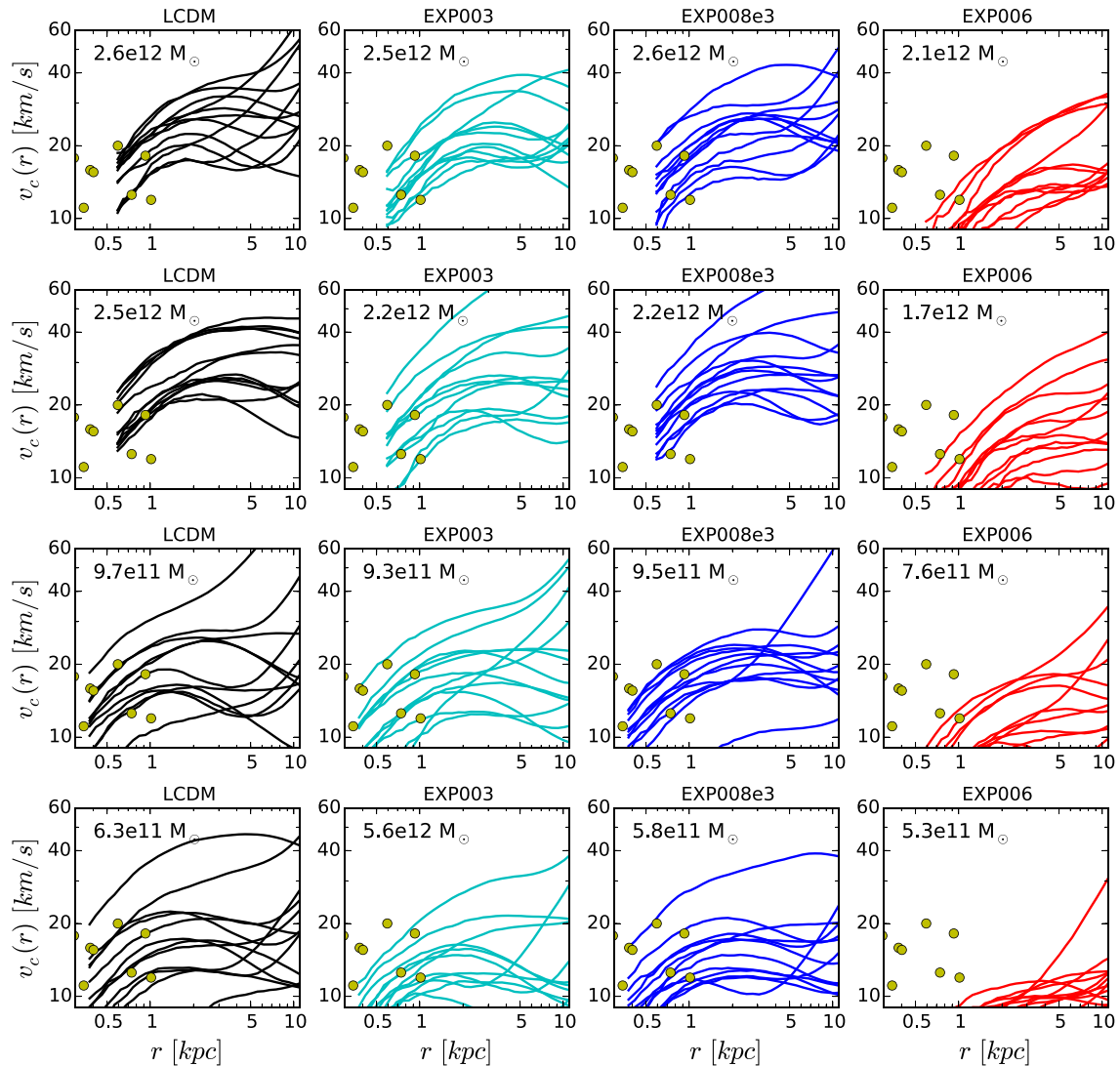


Figure 12. Rotation curves of the most massive subhaloes at the moment of infall for each halo in each cosmology. From the top row down we show halo α , halo β , halo γ , halo δ , from left to right we show Λ CDM (black), EXP003 (cyan), EXP008e3 (blues), EXP006 (red). We estimate the subhalo mass ranking at the moment of infall using the correlation between orbital energy and subhalo mass-loss found in Anderhalden et al. (2013). The yellow points are the observed values for $v_{\text{circ}}(r_{1/2})$ for the brightest dwarf galaxies orbiting around the Milky Way. Data are taken from Anderhalden et al. (2013) and references therein. The masses of each main halo realizations is written on each panel.

that alternative cosmologies can contribute to alleviate the tension between predictions and observations.

Fig. 12 shows the rotation curves for the 12 most massive subhaloes at the moment of infall. We used the correlation between orbital energy and subhalo mass-loss found in Anderhalden et al. (2013) to determine the subhaloes ranking. Each row illustrates subhaloes rotation curves for a given main halo in all considered cosmologies. From top down we show halo α , halo β , halo γ , halo δ . In yellow, we show the observed values for $v_{\text{circ}}(r_{1/2})$ for the brightest dwarf galaxies orbiting around the Milky Way, data are taken from Anderhalden et al. (2013) and references therein. Despite halo α and halo β having comparable masses, the tension between simulated curves and measured points in the Λ CDM case is more evident in halo β , supporting the fact that subhalo properties can vary even when host haloes have the same virial mass (Purcell & Zentner 2012). The tension is alleviated in the case of halo γ and even more halo δ , given their lower masses (Vera-Ciro et al. 2013). Overall, when looking at all haloes in EXP003 and EXP008e3 cos-

mologies, these do not show significant improvement compared to their Λ CDM realizations in decreasing the inner densities of subhaloes. On the other hand, in the case of EXP006 cosmology, all four haloes show such a dramatic decrease in subhaloes rotational velocity peaks that rotation curves become incompatible with measured values. The dramatic decrease was to be expected given the choice of a large coupling parameter for EXP006 cosmology, but none the less it is useful to understand the effects of the coupling.

4.3 Zooming-in on a dwarf halo

To better explore the effects of the coupling at high resolutions, we simulated a dwarf galaxy halo, halo ϵ . We chose an isolated halo (no structures with comparable mass within four of its virial radii) and, given the results of Section 4.2, we only focused on the two most distant cosmological cases, Λ CDM and EXP006 cosmology. The virial masses are 4×10^9 and $3 \times 10^9 M_{\odot}$ respectively, with a mass resolution of $1.3 \times 10^3 M_{\odot}$. Fig. 13 shows the density maps

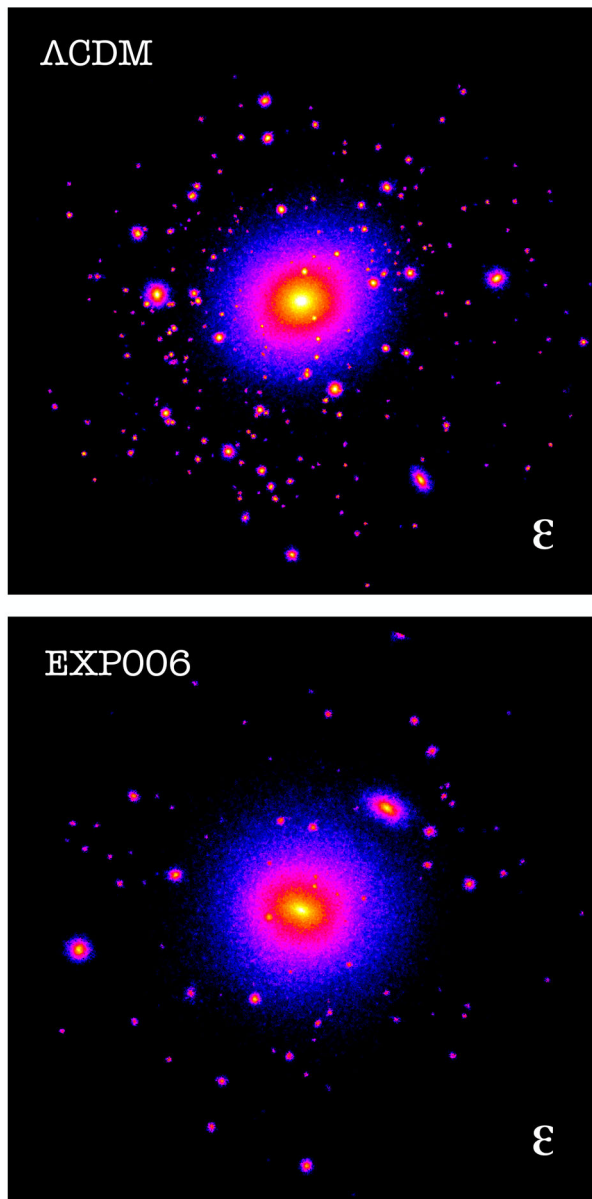


Figure 13. Density maps for halo ϵ in Λ CDM (upper panel) and in EXP006 cosmology (lower panel). The side of each projection is R_{200} .

for halo ϵ in both cosmologies, with Λ CDM on the upper panel. It is visible how the number of substructures decreases in the case with coupling. Upper panels of Fig. 14 show density profiles and rotation curves for halo ϵ in both cosmologies. The effect of the coupling is very evident in lowering the concentration and flattening the rotation curve. The values for the halo concentrations are $c = 15.2$ and 6.5 for Λ CDM and EXP006 cosmology, respectively. Although the density profile in the coupled dark energy case is less concentrated, it is still cuspy, showing that in coupled cosmologies, as in Λ CDM, we are not able to produce a dark matter only cored density profile. The inconsistency with observation thus still persists, given the observational evidence that supports cored density profiles for the satellites of the Milky Way (Walker & Peñarrubia 2011; Amorisco & Evans 2012; Amorisco, Agnello & Evans 2013). Interesting to note, by constructing a model in which both warm and cold dark matter are present and only the cold component is coupled to dark

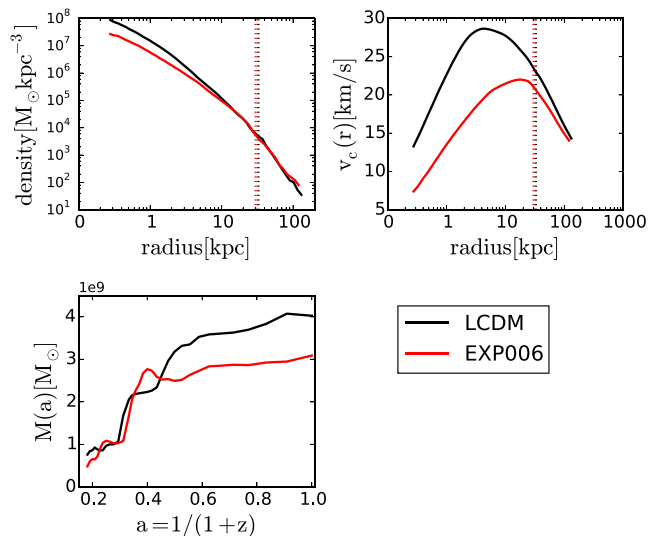


Figure 14. Upper left and right panels show density profiles and rotation curves for halo ϵ in Λ CDM (black) and in EXP006 (red) cosmology. The inner minimum radius is three times the softening length, while the most outer radius is four times R_{200} . The vertical dashed lines represent R_{200} for each cosmology. Lower panel shows the accretion history for halo ϵ for Λ CDM and EXP006 cosmologies.

energy, a very high value ($\beta_c \sim 10$) for the coupling constant is favoured (Bonometto, Mainini & Macciò 2015) and simulated dark matter only dwarf haloes show a cored density profile (Macciò et al. 2015). The lower panel of Fig. 14 shows the accretion history, M_{200} as function of scale factor. As in Section 4.1.3, we calculated the formation epochs referring to the scale factor at which the halo has gained half of its today's mass. We find $a_c = 0.331$ (Λ CDM), $a_c = 0.329$ (EXP006). Despite the very significant difference in concentration between these two haloes, their formation times are comparable, confirming that the difference in concentration is not driven by formation times but rather by the modified dynamics, also at dwarf galaxy scales.

5 CONCLUSIONS

We have performed the first study of high-resolution galactic scale simulations in coupled dark energy cosmologies. The aim is to study the effects of the coupling between dark energy and dark matter on these scales, so far neglected in previous studies. We chose to investigate two models with coupling values that are within the observational constraints from Pettorino et al. (2012), one with constant coupling and one with varying coupling with redshift; we also chose a third model where the constant coupling value has been pushed beyond observational constraints to better investigate its effects. We then selected three Milky Way-sized haloes, a $6 \times 10^{11} M_\odot$ halo and a dwarf halo $5 \times 10^9 M_\odot$, and studied their properties in a Λ CDM reference model and in the coupled cosmologies, resolving each halo with $\sim 10^6$ dark matter particles.

We computed concentrations and formation epochs for all haloes and we find that, despite the earlier or comparable formation epochs of the coupled cosmologies haloes, these have lower concentrations. In a Λ CDM or a dynamical dark energy scenario, earlier formation epochs would imply higher concentrations, but in the coupled dark energy case the reason for lower concentrations is not related to formation histories, but rather to the modified dynamics. We ascribe this behaviour to the presence of the friction term $-\beta\dot{\phi}\delta_c$ in the

equation for the linear evolution of density perturbations (equation 4) in coupled cosmologies. This extra term, compared to the Λ CDM case, redistributes the dark matter particles and lowers the central densities, in spite of the formation times (see Baldi 2011b). Given that the mass range that we investigate is complementary to previous studies, we cannot exclude that also other extra terms appearing with the coupling can be important.

In particular, subhaloes can also be significantly less concentrated. When falling towards their host, they can be more heavily stripped once they start feeling the gravitational influence of the host halo. One possible explanation is that this translates into decreasing the number of subhaloes compared to the Λ CDM realization and, additionally, subhaloes are themselves less massive and less concentrated. For these reasons, coupled cosmologies can be helpful in alleviating satellite-scales inconsistencies of Λ CDM. On the other hand, we find that in order to try to solve these issues with the coupling alone, one needs to use an extreme value for the coupling constant that is ruled out by observational constraints. In fact, only in the case with the highest coupling value the number of subhaloes is significantly reduced (up to 75 per cent less subhaloes) than in the respective Λ CDM cases, while for the viable coupling cosmologies the decrease is much less significant (10 per cent less subhaloes). Moreover, we find that the distribution of the subhaloes inside the main halo virial radius does not vary significantly among cosmologies. Lastly, less concentrated coupled cosmologies subhaloes can in principle be useful to reconcile the inconsistency between the observed properties of the Milky Way dwarf galaxies and Λ CDM simulations predictions, but once more a high enough value for the coupling must be assumed. Interestingly, allowing the introduction of massive neutrinos does alleviate the constraints on the coupling (see e.g. La Vacca et al. 2009), leaving coupled dark energy models dynamics an interesting option for subgalactic scales.

Overall coupled dark energy models can be as effective as Λ CDM in reproducing observations on subgalactic scales. Furthermore, by increasing the coupling value, these models may help improve the agreement between predicted and observed properties. Given that higher coupling becomes viable when considering other extensions to the Λ CDM model, coupled dark energy models present themselves as an interesting alternative to the standard model. These cosmologies would need to be further investigated, possibly taking into account the effects of baryons at subgalactic scales, which, as already shown in dynamical dark energy models (Penzo et al. 2014), are expected to amplify differences observed in the dark matter only case.

ACKNOWLEDGEMENTS

CP is supported by postdoctoral funding from ERC-StG ‘EDECS’ no. 279954. The numerical simulations were performed on the THEO cluster of the Max-Planck-Institut für Astronomie and HYDRA cluster, both based at the Rechenzentrum in Garching. CP and AVM acknowledge the support from the Sonderforschungsbereich SFB 881 ‘The Milky Way System’ (subproject A02) of the German Research Foundation (DFG). CP also acknowledges the support of the International Max Planck Research School, Heidelberg (IMPRS-HD). MB acknowledges partial support by the Marie Curie Intra European Fellowship ‘SIDUN within the 7th Framework Programme of the European Commission. LC acknowledges the Brazilian research Institutions FAPES and CNPq for financial support.

REFERENCES

- Agnello A., Evans N. W., 2012, *ApJ*, 754, L39
 Alam S. et al., 2015, *ApJS*, 219, 12
 Amendola L., 2000, *Phys. Rev. D*, 62, 043511
 Amendola L., 2004, *Phys. Rev. D*, 69, 103524
 Amendola L., Tocchini-Valentini D., 2001, *Phy. Rev. D*, 64, 043509
 Amendola L., Gasperini M., Piazza F., 2004, *J. Cosmol. Astropart. Phys.*, 9, 14
 Amorisco N. C., Evans N. W., 2012, *MNRAS*, 419, 184
 Amorisco N. C., Agnello A., Evans N. W., 2013, *MNRAS*, 429, L89
 Anderhalden D., Diemand J., Bertone G., Macciò A. V., Schneider A., 2012, *J. Cosmol. Astropart. Phys.*, 10, 47
 Anderhalden D., Schneider A., Macciò A. V., Diemand J., Bertone G., 2013, *J. Cosmol. Astropart. Phys.*, 3, 14
 Anderson G. W., Carroll S. M., 1998, in Roszkowski L., ed., *COSMO-97, First International Workshop on Particle Physics and the Early Universe*. World Scientific Press, Singapore, p. 227
 Baldi M., 2011a, *MNRAS*, 411, 1077
 Baldi M., 2011b, *MNRAS*, 414, 116
 Baldi M., Pettorino V., Robbers G., Springel V., 2010, *MNRAS*, 403, 1684
 Bertschinger E., 2001, *ApJS*, 137, 1
 Billyard A. P., Coley A. A., 2000, *Phy. Rev. D*, 61, 083503
 Bonometto S. A., Mainini R., Macciò A. V., 2015, *MNRAS*, 453, 1002
 Boylan-Kolchin M., Bullock J. S., Kaplinghat M., 2011, *MNRAS*, 415, L40
 Brooks A. M., Zolotov A., 2014, *ApJ*, 786, 87
 Carlesi E., Knebe A., Lewis G. F., Wales S., Yepes G., 2014, *MNRAS*, 439, 2943
 Di Cintio A., Brook C. B., Macciò A. V., Stinson G. S., Knebe A., Dutton A. A., Wadsley J., 2014, *MNRAS*, 437, 415
 Diemand J., Zemp M., Moore B., Stadel J., Carollo C. M., 2005, *MNRAS*, 364, 665
 Dolag K., Bartelmann M., Perrotta F., Baccigalupi C., Moscardini L., Meneghetti M., Tormen G., 2004, *A&A*, 416, 853
 Dutton A. A., Macciò A. V., 2014, *MNRAS*, 441, 3359
 Farrar G. R., Peebles P. J. E., 2004, *ApJ*, 604, 1
 Flores R. A., Primack J. R., 1994, *ApJ*, 427, L1
 Gentile G., Famaey B., Zhao H., Salucci P., 2009, *Nature*, 461, 627
 Governato F. et al., 2012, *MNRAS*, 422, 1231
 Gromov A., Baryshev Y., Teerikorpi P., 2004, *A&A*, 415, 813
 Guo Z.-K., Ohta N., Tsujikawa S., 2007, *Phy. Rev. D*, 76, 023508
 Jones D. H. et al., 2009, *MNRAS*, 399, 683
 Kennedy R., Frenk C., Cole S., Benson A., 2014, *MNRAS*, 442, 2487
 Klypin A., Kravtsov A. V., Valenzuela O., Prada F., 1999, *ApJ*, 522, 82
 Klypin A., Macciò A. V., Mainini R., Bonometto S. A., 2003, *ApJ*, 599, 31
 Knollmann S. R., Knebe A., 2009, *ApJS*, 182, 608
 Koivisto T., 2005, *Phy. Rev. D*, 72, 043516
 La Vacca G., Kristiansen J. R., Colombo L. P. L., Mainini R., Bonometto S. A., 2009, *J. Cosmol. Astropart. Phys.*, 0904, 007
 Lewis A., Bridle S., 2002, *Phys. Rev. D*, 66, 103511
 Li B., Barrow J. D., 2011, *Phys. Rev. D*, 83, 024007
 Lovell M. R. et al., 2012, *MNRAS*, 420, 2318
 Ludlow A. D. et al., 2013, *MNRAS*, 432, 1103
 Macciò A. V., Quercellini C., Mainini R., Amendola L., Bonometto S. A., 2004, *Phy. Rev. D*, 69, 123516
 Macciò A. V., Dutton A. A., van den Bosch F. C., 2008, *MNRAS*, 391, 1940
 Macciò A. V., Kang X., Fontanot F., Somerville R. S., Koposov S., Monaco P., 2010, *MNRAS*, 402, 1995
 Macciò A. V., Mainini R., Penzo C., Bonometto S. A., 2015, *MNRAS*, 453, 1371
 Madau P., Diemand J., Kuhlen M., 2008, *ApJ*, 679, 1260
 Mangano G., Miele G., Pettorino V., 2003, *Mod. Phys. Lett. A*, 18, 831
 Matarrese S., Pietroni M., Schimd C., 2003, *J. Cosmol. Astropart. Phys.*, 8, 5
 Moore B., 1994, *Nature*, 370, 629
 Moore B., Ghigna S., Governato F., Lake G., Quinn T., Stadel J., Tozzi P., 1999, *ApJ*, 524, L19
 Navarro J. F., Frenk C. S., White S. D. M., 1997, *ApJ*, 490, 493

- Oñorbe J., Boylan-Kolchin M., Bullock J. S., Hopkins P. F., Kereš D., Faucher-Giguère C.-A., Quataert E., Murray N., 2015, *MNRAS*, 454, 2092
- Peebles P. J. E., Ratra B., 1988, *ApJ*, 325, L17
- Penzo C., Macciò A. V., Casarini L., Stinson G. S., Wadsley J., 2014, *MNRAS*, 442, 176
- Perlmutter S. et al., 1999, *ApJ*, 517, 565
- Pettorino V., Amendola L., Baccigalupi C., Quercellini C., 2012, *Phy. Rev. D*, 86, 103507
- Planck Collaboration XIII, 2015, preprint ([arXiv:1502.01589](https://arxiv.org/abs/1502.01589))
- Purcell C. W., Zentner A. R., 2012, *J. Cosmol. Astropar. Phys.*, 12, 7
- Rashkov V., Madau P., Kuhlen M., Diemand J., 2012, *ApJ*, 745, 142
- Riess A. G. et al., 1998, *AJ*, 116, 1009
- Salucci P., Wilkinson M. I., Walker M. G., Gilmore G. F., Grebel E. K., Koch A., Frigerio Martins C., Wyse R. F. G., 2012, *MNRAS*, 420, 2034
- Simon J. D., Bolatto A. D., Leroy A., Blitz L., Gates E. L., 2005, *ApJ*, 621, 757
- Springel V., 2005, *MNRAS*, 364, 1105
- Swaters R. A., Madore B. F., van den Bosch F. C., Balcells M., 2003, *ApJ*, 583, 732
- Tollerud E. J., Beaton R. L., Geha M., Guhathakurta P., Bullock J. S., Kalirai J. S., Kirby E. N., Boylan-Kolchin M., 2012, *BAAS*, 219, 201.04
- van den Bosch F. C., Swaters R. A., 2001, *MNRAS*, 325, 1017
- Vera-Ciro C. A., Helmi A., Starkenburg E., Breddels M. A., 2013, *MNRAS*, 428, 1696
- Vogelsberger M., Zavala J., Loeb A., 2012, *MNRAS*, 423, 3740
- Walker M. G., Peñarrubia J., 2011, *ApJ*, 742, 20
- Wechsler R. H., Bullock J. S., Primack J. R., Kravtsov A. V., Dekel A., 2002, *ApJ*, 568, 52
- Weinberg S., 1989, *Rev. Mod. Phys.*, 61, 1
- Wetterich C., 1988, *Nucl. Phys. B*, 302, 668
- Wetterich C., 1995, *A&A*, 301, 321
- Zimdahl W., Pavón D., Chimento L. P., 2001, *Phys. Lett. B*, 521, 133

This paper has been typeset from a $\text{\TeX}/\text{\LaTeX}$ file prepared by the author.